Influence of Mechanical Couplings on the Buckling and Postbuckling of Anisotropic Plates

David W. Jensen* and Paul A. Lagace†
Massachusetts Institute of Technology, Cambridge, Massachusetts

An experimental and analytical investigation was conducted on the buckling and postbuckling behavior of generally anisotropic graphite/epoxy laminated plates. The elastic (mechanical) couplings inherent in unbalanced and unsymmetric laminates have been isolated, including bending-stretching, the stretching-shearing and bending-twisting combination, and stretching-twisting coupling. Laminates with a 254 mm square test section were manufactured from Hercules AS4/3501-6 graphite/epoxy and tested in uniaxial compression to failure with clamped and simply supported sides. Rayleigh-Ritz and finite-element linear analytical solutions were used to predict the buckling loads and mode shapes. The Rayleigh-Ritz analysis was extended to the nonlinear regime by introducing von Kármán's large deflection strain-displacement relations to predict the compressive postbuckling (prefailure) behavior. The results show that the introduction of elastic couplings reduces the buckling loads, although the concept of bifurcation cannot be clearly applied to unsymmetric laminates.

Nomenclature

a	= plate length in x direction
$[A]$	= elastic stretching matrix
b	= plate width in y direction
$[B]$	= elastic coupling matrix
$[D]$	= elastic bending matrix
F_k	= vibrating beam functions
$[K]$	= stiffness matrix
$[L]$	= loading matrix
N_{cr}	= critical buckling load resultant
N_x	= applied load resultant in x direction
P	= applied load
q_i	= generalized displacements
U	= total strain energy
U_i	= components of strain energy
u,v,w	= displacements in the x,y,z directions
W	= work done by external forces
w_c	= assumed deflection for clamped sides
w_{ss}	= assumed deflection for simply-supported sides
x,y,z	= plate coordinates
$\{\varepsilon^0\}$	= strain vector at laminate midplane
$\{\kappa\}$	= curvature vector
Π_p	= total potential energy

I. Introduction

THE use of advanced composite materials in modern aerospace structures provides the designer with the ability to achieve significant weight reductions for given structural requirements of stiffness and strength as well as critical performance advantages. However, these laminated materials also present a challenge in the design process since elastic couplings are introduced into the mechanical behavior, which require more careful analysis than is usually necessary for traditional isotropic and orthotropic plates.[1] For example, the use of unbalanced laminates to aeroelastically tailor the response of a wing[2] and provide performance advantages[3] is achieved via the couplings between the bending and twisting behavior of a laminate as well as between the in-plane stretching and shearing.

This complexity increases further if unsymmetric laminates are employed, since the stretching (membrane) and bending (flexural) response are coupled. This can result in fully anisotropic structural behavior insofar as the bending, stretching, shearing, and twisting responses become completely coupled. These unsymmetric laminates arise "naturally" in the design process, such as at locations where plies are dropped off in a panel in order to taper the thickness. These plies are generally dropped off in an unsymmetric fashion due to design constraints. Furthermore, the local delamination of plies or sublaminates, such as due to an impact event,[4] in an otherwise symmetric laminate can also create local unsymmetric sublaminates that can affect the residual strength and stiffness of a structure. There also may be applications where the unique couplings inherent in unsymmetric laminates provide design advantages.

An understanding of the behavior of these laminates in compressive loading, specifically their buckling and postbuckling characteristics, is important since many structural components undergo significant compressive loads. A comprehensive summary of the current state-of-the-art in buckling and postbuckling of composites has been recently compiled by Leissa[5] with a review of almost 400 works performed in the past few decades. Although most of these works deal with symmetric, balanced composite plates, some work[6-8] has been conducted on unsymmetric laminates. It has been demonstrated that the elastic couplings inherent in these laminates reduce the structural stiffness resulting in lower buckling loads and generally more compliant behavior. These works have generally, however, been limited to the linear buckling problem of laminates. Recently, an invaluable collection of analytical work on the nonlinear analysis of plates, including applications to the postbuckling of unsymmetric composite plates, has been assembled by Chia.[9]

The influence of these elastic couplings mandates reconsideration of the concept of bifurcation buckling for unsymmetric laminates. The mechanical behavior of such laminates is somewhat analogous to that of plates with an initial curvature or

Received March 6, 1986; revision received Feb. 6, 1988.

*Technology Laboratory for Advanced Composites, Department of Aeronautics and Astronautics; currently Assistant Professor of Aerospace Engineering, Pennsylvania State University. Member AIAA.

†Associate Professor of Aeronautics and Astronautics, Technology Laboratory for Advanced Composites, Department of Aeronautics and Astronautics. Member AIAA.

loaded eccentrically insofar as the out-of-plane deflections begin simultaneously with the application of load.[8] The shifting of the neutral bending surface from the center in laminates with couplings significantly reduces the critical buckling load. However, generally unsymmetric laminates may not possess any definable neutral surface due to the existence of membrane-flexural couplings, and thus the concept of initial buckling is not as clear. It therefore becomes even more important to investigate the postbuckling, or nonlinear response, of these plates. Furthermore, conventional aircraft wing panels are often designed to operate in this postbuckled region. Thus, a full understanding of the compressive response of these laminates is mandated.

II. Methodology

This research effort consisted of an experimental and analytical investigation into the general buckling and postbuckling behavior of unbalanced and unsymmetric laminated graphite/epoxy plates. It builds on previous work conducted and reported by the authors[8] where the basic experimental techniques were developed and a preliminary buckling analysis was performed. In the part of the investigation reported herein, a total of 28 laminated plates of five different stacking sequences were manufactured and tested.

The general category of membrane-flexural coupling includes stretching-bending, stretching-twisting, and shearing-twisting couplings. The laminates used in this investigation were chosen in order to isolate these various couplings. Bending-stretching coupling is isolated in an antisymmetric orthotropic laminate $[0_3//90_3//0_3//90_3]_T$. Stretching-twisting coupling is isolated in an unsymmetric but balanced laminate $[0_2//45_2//0_2//-45_2//0_2]_T$, whereas the combination of stretching-shearing and bending-twisting is inherent in the symmetric and unbalanced construction of the $[0_2//45_2//0_2//45_2//0_2]_T$ laminate. The subscript T indicates that this is a total laminate, in order to distinguish these from a symmetric arrangement. The double slash // indicates a room temperature bondline joining previously cured symmetric sublaminates. This type of construction[8] was necessary in order to obtain flat unsymmetric laminates.

In addition to the unsymmetric laminates, a basic specially orthotropic laminate that does not exhibit any couplings, $[0_3/90_3]_s$, was chosen to serve as a benchmark. A $[0_3//90_3//90_3//0_3]_T$ laminate, which has the same number of plies and stacking sequence but uses the room temperature bondline construction, was also included to ascertain the effects of this bondline.

The plates were tested in uniaxial compression with clamped or simply supported side boundary conditions and clamped-loaded ends. A summary of the test matrix is presented in Table 1. Load, out-of-plane deflection, and strain data were obtained experimentally. Free side boundary conditions were also considered, but their results behaved according to classical wide-column theory[10] and are the subject of another communication.

Two different theoretical techniques were implemented to predict the buckling loads and mode shapes, and the postbuckling behavior of the plates studied herein. One analysis is based on the Rayleigh-Ritz assumed modes energy method involving a direct minimization of the total potential energy of the system. The Rayleigh-Ritz method provides significant insight into the fundamental mechanisms that govern the compressive behavior of unsymmetric laminated plates and is further useful in preliminary design. The other analysis is a finite-element formulation performed using a 32-degree-of-freedom (DOF) hybrid semi-Loof element developed recently for the express application of thin composite plates and shells.[11,12] The finite-element method was used to verify that the modes selected for the Rayleigh-Ritz analysis could adequately model the complex behavior. Linear analyses were performed using these two techniques to predict the critical buckling loads and mode shapes. An extension of the Rayleigh-Ritz analysis was used to predict the postbuckling, which is large displacement and thus nonlinear behavior.

Table 1 Test matrix

Laminate	Side boundary conditions: Clamped	Side boundary conditions: Simply supported
$[0_3/90_3]_s$	3[a]	1
$[0_3//90_3//90_3//0_3]_T$	5	1
$[0_3//90_3//0_3//90_3]_T$	5	1
$[0_2//45_2//0_2//45_2//0_2]_T$	5	1
$[0_2//45_2//0_2//-45_2//0_2]_T$	5	1

[a]Indicates number of specimens tested.

III. Analytical Techniques

A. Rayleigh-Ritz

For a general laminated composite plate, the internal potential energy can be expressed in terms of the elastic matrices from the constitutive relations as

$$U = \frac{1}{2}\iint [\{\varepsilon^0\}^T[A]\{\varepsilon^0\} + 2\{\varepsilon^0\}^T[B]\{\kappa\} + \{\kappa\}^T[D]\{\kappa\}]\,dx\,dy \tag{1}$$

The analytical formulation is generalized by introducing von Kármán's nonlinear strain-displacement relations[13] into the expression for the potential energy resulting in a lengthy equation, which can be expressed as the sum of six parts:

$$U = \sum_{i=1}^{6} U_i \tag{2}$$

The first three components, U_1, U_2, and U_3, are the linear terms used in both the linear buckling analysis and the nonlinear postbuckling analysis. The remaining three components, U_4, U_5, and U_6, represent the nonlinear contributions to the strain energy and provide the essential information for the large deflection postbuckling analysis. It should be noted that the U_2 and U_5 terms are unique to unsymmetric laminates in that they contain components of the B matrix, which characterize the membrane-flexural coupling. These individual terms are not shown herein for the sake of brevity but can be found in Ref. 10.

The work performed on the plate by the external forces must also be accounted for. The work expression for the case of a thin plate loaded in uniaxial compression N_x, as illustrated in Fig. 1, takes the form

$$\delta W = \delta \int N_x u(a,y)\,dy = -\frac{1}{2}\delta \iint N_x \left(\frac{\partial w}{\partial x}\right)^2 dx\,dy \tag{3}$$

The first part of this expression was employed in the nonlinear analysis. For the linear analysis, the latter equivalent expression for the work was used to facilitate the ensuing eigenvalue problem.

The most critical step in the Rayleigh-Ritz analysis is the selection of assumed modes. The operating assumption is that the behavior can be adequately modeled by a series of separable displacement functions for the deflections u, v, and w. Linear combinations of components from both geometric and trigonometric series were chosen to represent each of the displacements.

A total of 21 modes were used to represent the deflection in the x direction:

$$u = q_1\left(\frac{x}{a}\right) + \sum_{n=1}^{4} q_{n+17}\left(\frac{x}{a} - \frac{1}{2}\right)\cos\left(\frac{n\pi y}{b}\right) + \sum_{m=1}^{4}\sum_{n=1}^{4} q_{4(m-1)+n+1}\sin\left(\frac{m\pi x}{a}\right)\cos\left(\frac{[2n-1]\pi y}{b}\right) \quad (4)$$

and a total of 22 modes were used to represent the deflection in the y direction:

$$v = q_{22}\left(\frac{y}{b}\right) + q_{23}\left(\frac{x}{a}\right) + \sum_{m=1}^{4} q_{m+39}\cos\left(\frac{m\pi x}{a}\right)\left(\frac{y}{b} - \frac{1}{2}\right) + \sum_{m=1}^{4}\sum_{n=1}^{4} q_{4(m-1)+n+23}\cos\left(\frac{m\pi x}{a}\right)\sin\left(\frac{[2n-1]\pi y}{b}\right) \quad (5)$$

The assumed modes for the deflection in the z direction are dependent on the side boundary conditions. For the clamped case

$$w_c = \sum_{m=1}^{3}\sum_{n=1}^{3} q_{3(m-1)+n+43} F_m\left(\frac{x}{a}\right)F_n\left(\frac{y}{b}\right) \quad (6)$$

were used, whereas the assumed form for the simply supported case was

$$w_{ss} = \sum_{m=1}^{3}\sum_{n=1}^{3} q_{3(m-1)+n+43} F_m\left(\frac{x}{a}\right)\sin\left(\frac{n\pi y}{b}\right) \quad (7)$$

In these assumed forms for w, the F_k represent standard vibrating beam functions:[14]

$$F_k = \cosh\left(\frac{\alpha_k x}{a}\right) - \cos\left(\frac{\alpha_k x}{a}\right) - \gamma_k\left[\sinh\left(\frac{\alpha_k x}{a}\right) - \sin\left(\frac{\alpha_k x}{a}\right)\right] \quad (8)$$

These modes were carefully chosen to ensure that the complex buckling patterns and large displacement behavior were properly represented. Particular attention was paid to allow for the full effects of the coupling between the in-plane extension and shear, and the out-of-plane bending and twisting in addition to the membrane-flexural coupling. A complete description of this formulation is provided in Ref. 10.

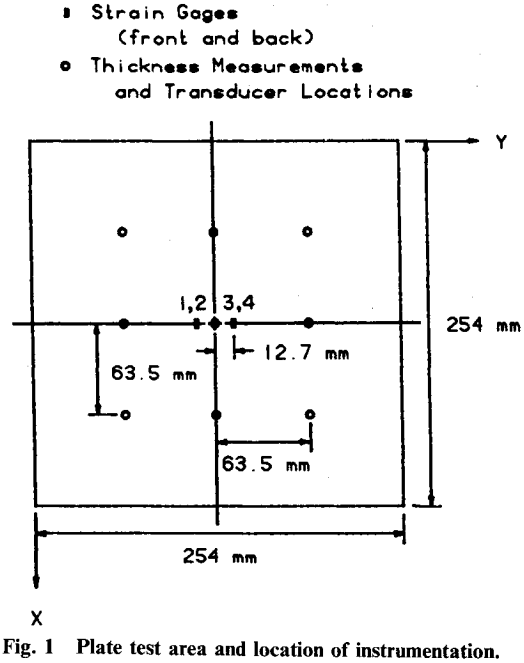

Fig. 1 Plate test area and location of instrumentation.

1. Linear Problem

The linear stability problem is solved by invoking the principle of stationary potential energy:

$$\delta\Pi_p = 0 \quad (9)$$

which, for the linear problem, is simplified to

$$\delta\Pi_p = \delta\sum_{i=1}^{3} U_i - \delta W \quad (10)$$

The assumed displacement functions are placed into the expression for the total potential energy, and the minimization yields a standard eigenvalue problem:

$$[K]\{q\} = N_{cr}[L]\{q\} \quad (11)$$

where $[K]$ and $[L]$ are the resulting stiffness and loading matrices. This is solved for the eigenvalue N_{cr}, which is the critical load resultant applied in the x direction to cause bifurcation buckling.

It was previously noted that for unsymmetric laminates, a true bifurcation does not manifest itself experimentally. It is, therefore, difficult at best to experimentally establish an appropriate criterion for the determination of the critical buckling load. However, a pseudo-elastic buckling load can be determined from experimental load-deflection curves using the method developed by Southwell.[15] This will serve as a comparative parameter, and thus the calculation of the theoretical bifurcation buckling load is useful. Furthermore, the deflection modes determined from the linear analysis can be compared with the deflection shapes determined experimentally.

2. Nonlinear Problem

The solution procedure for the full nonlinear problem is based on a direct minimization of the total potential energy of the system for any given load using a structural optimization search technique.[16] The nonlinear equations were solved using a modified Newton-Raphson iterative solution method. This method was selected because it ensures rapid convergence at each iteration. However, it requires inverting the Jacobian matrix at each step, and thus it is primarily applicable to problems with only a few degrees of freedom.

Beginning with the linear solutions for the displacements, based on the lowest few natural buckling modes, the corresponding local minima are determined using the full nonlinear equations. An iterative procedure is used until the desired convergence is achieved for each local minimum. The entire procedure is repeated for each of the lowest few modes. The resulting local minima are then compared in order to ascertain which solution represents the global minimum of the energy functional.

For the nonlinear problem, the influence of lateral spring forces was included to model the effect of the out-of-plane deflection measurement transducers used in the experiment (as described in the experimental section). This involves an additional term due to the energy stored in these springs as well as a term due to the work done by these springs. The small values of the transducer spring constants are negligible in magnitude when compared to the bending stiffness of the plate and, therefore, do not affect the bifurcation buckling load. Thus, these transducers were neglected in the linear problem.

The nonlinear analysis was performed at various discrete loads, and the deflections of the plate were determined at these loads. Analytical plots of load vs deflection were then constructed and compared with those determined experimentally.

3. Implementation

Both the linear and nonlinear analyses were implemented using double precision FORTRAN programs on a VAX 11/782. The nondimensional integrations were performed using a second-order Newton-Cotes integration technique with 21 integration steps.

B. Finite-Element Analysis

A 32-DOF hybrid semi-Loof plate element[11,12] with 37 independent stress parameters based on an extended Hellinger-Reissner principle was used in this investigation. The laminated plates were analyzed using a 5 × 5 grid, as shown in Fig. 2, for a total of 408 DOF. As with the linear Rayleigh-Ritz analysis, the linear finite-element method reduces to a standard eigenvalue problem that can be solved for the critical buckling load using standard eigenvalue solution techniques.

IV. The Experiment

Most of the plates listed in Table 1 were manufactured in a two-part operation. The first part involved the preparation of 305 mm × 350 mm symmetric (and unidirectional) sublaminates from Hercules AS4/3501-6 graphite/epoxy using standard procedures. The plates were cured in an autoclave under 0.59 MPa pressure and 762 mm Hg vacuum with a one-hour hold at 116°C and a two-hour hold at 177°C. After an eight-hour postcure at 177°C, the sublaminates were machined to 292 mm square using a milling machine equipped with a diamond-grit cutting wheel and water cooling. Thickness measurements taken at the nine locations corresponding to the positions where deflection data would be recorded, as noted in Fig. 1, indicated excellent quality. The manufacturer's nominal per ply thickness of 0.134 mm was used for all calculations.

The second part of the manufacturing process involves bonding the prepared sublaminates to the desired configuration using a room temperature cure system, Dexter HYSOL EA 956 low-viscosity adhesive. The laminates were bonded in the autoclave under 0.52 MPa pressure and 762 mm Hg vacuum at 25°C. The pressure was maintained for two hours and the vacuum for 24 hours after which the laminates were machined to their final dimensions of 279 mm square. Repeated thickness measurements indicated an average bondline thickness in the vicinity of 0.03 mm. This value was used in all calculations. The important properties of the graphite/epoxy and adhesive that were used are summarized in Table 2. Prior to testing, each of the plates was instrumented with two pairs of Micro Measurements EA-06-125AC-350 strain gages mounted back-to-back in the positions illustrated in Fig. 1.

In order to observe the buckling and postbuckling behavior of the selected laminates, a monotonically increasing uniform compressive displacement of 0.42 mm/min was applied while measurements of the load, strains, end-shortening, and lateral deflections were sampled. The specimens were tested using a modular steel jig with interchangeable boundary conditions, used and verified in previous work,[8] in a 445 kN MTS 810 hydraulic testing machine. All sliding surfaces were lubricated with a molybdenum-lithium compound to reduce friction. The introduction of extraneous shear was minimized by applying layers of teflon tape to the borders of each plate and only loosely clamping the boundary constraints.[17] This resulted in a square test area of 254 mm to a side, as noted in Fig. 1.

Two types of lateral deflection measurements were obtained. The first type used a manually operated, 2-DOF scanning system mounted on the front of the loading jig.[8] This deflection tracker allowed mapping of the deflection pattern over the entire plate to be performed at discrete load levels. Isodeflection contour maps were generated from this data obtained using a 9 × 9 (internal) grid with 25 mm spacing from these scans. These data were supplemented by continuous out-of-plane deflection data taken at nine discrete locations using an array of gaging transducers. A modular cart assembly[10] employed six ±25 mm and three ±51 mm (in the center row) gaging transducers spaced 64 mm apart forming a 3 × 3 square grid, as shown in Fig. 1. An intricate procedure to assure

Table 2 Engineering constants of materials utilized

Property	Material: AS4/3501-6 Graphite/epoxy	Material: HYSOL EA956 Adhesive
E_L, GPa	139.3	1.7
E_T, GPa	11.14	1.7
G_{LT}, GPa	4.90	0.65
υ_{LT}	0.3	0.3

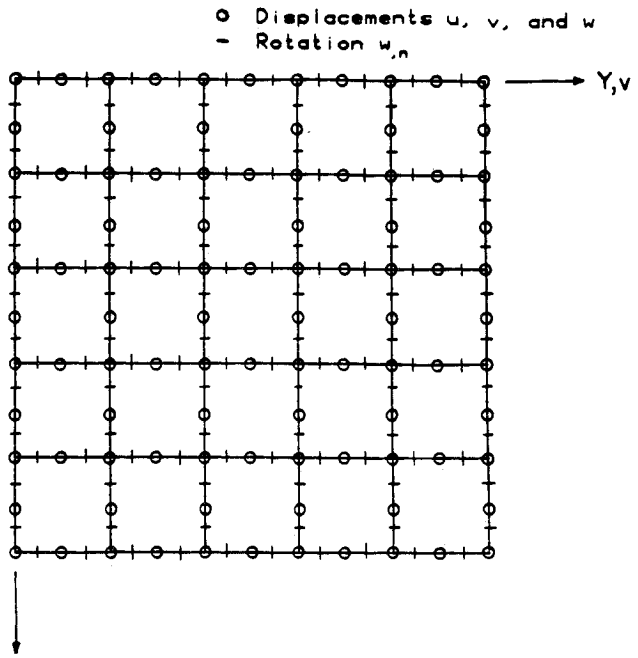

Fig. 2 Finite-element grid.

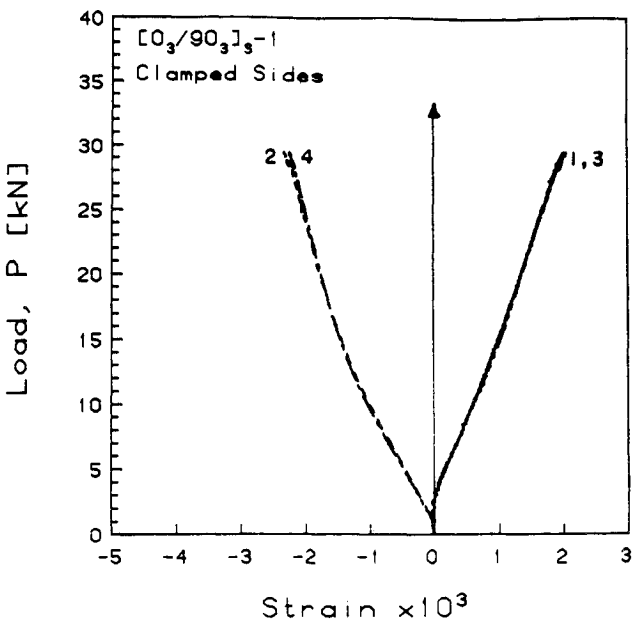

Fig. 3 Experimental stress-strain plot for $[0_3/90_3]_s$ specimen with clamped sides.

proper alignment of the jig and the plate within the jig was devised and used in the testing. This procedure is fully described in Ref. 10.

Once the plate was properly aligned, the load was applied until the deflection at the center of the plate was equal to one-half of the plate thickness. (It has previously been shown[18] that buckling has already taken place before this point.) A scan of the plate was taken at this point. For the first specimen of each type, the plate was subsequently unloaded and then reloaded to failure monotonically, where failure was defined by a sudden drop in load of 30% or greater.

The data from the first specimen of each laminate type gave indications as to the loads at which interesting mode shapes developed. In subsequent tests, loading was halted in order to perform a complete scan of the laminate at these loads.

V. Results and Implications

A. Initial Behavior

The stress-strain curves for all of the laminates exhibited an initially slow divergence of the readings from the back-to-back gages, which increased as the load increased. A typical plot is shown in Fig. 3. This indicates that out-of-plane deflections begin with the onset of load.

To compare these measurements with those anticipated, an effective modulus parameter has been defined.[8] An anisotropic plate has an undefinable elastic axis due to the existence of different B matrix couplings, and thus the definition of the longitudinal modulus is arbitrary in terms of the axis system and centerline chosen. The parameter used herein is the ratio of the applied load resultant N_x to the longitudinal strain at the laminate midplane ε_x^0, which experimentally is the average of the two readings of a back-to-back strain gage pair. For each of the laminates tested, the linear regions at the beginning of the load-strain curves were analyzed to determine this effective modulus parameter. These ratios, summarized in Table 3 along with the theoretical predictions, possess a fairly large coefficient of variation for each laminate set, as well as an inconsistency with the analytical predictions.

Table 3 Effective modulus parameter[a] N_x/ε_x^0

	Experimental[a]		
Laminate	Clamped[b]	S.S.[b]	Theoretical
$[0_3/90_3]_s$	93(27%)[c]	95[d]	122
$[0_3//90_3//90_3//0_3]_T$	83(16%)	68[d]	122
$[0_3//90_3//0_3//90_3]_T$	67(8.3%)	59[d]	105
$[0_2//45_2//0_2//45_2//0_2]_T$	72(10%)	80[d]	121
$[0_2//45_2//0_2//-45_2//0_2]_T$	75(19%)	71[d]	121

[a]All values in kN/mm.
[b]Side boundary conditions.
[c]Numbers in parentheses are coefficients of variation.
[d]Only one specimen tested with simply supported sides.

Two major factors contribute to these discrepancies. First, the couplings inherent in the laminates studied induce internal stresses and moments other than the applied axial load resultant N_x, which would cause shearing, bending, and twisting if the plate was not physically restrained. However, the presence of the boundary conditions restricts this motion by exerting additional reactive forces and moments. Such effects are not included in the simple analytical predictions for this parameter, which are based on the constitutive relations of classical laminated plate theory. Second, due to the manner in which the specimens are loaded, the plates actually experience a uniform end-shortening during loading, as opposed to a uniform load distribution. As the plate deflects, the compliance across the plate changes, thus altering the actual load distribution. This is not accounted for in the derivation of this parameter.

End-shortening displacement measurements taken should compensate for this nonuniform stress distribution, since they represent an equivalent average strain over the entire plate. However, these data were extremely sensitive to miscellaneous compliance in the system, such as slight rotations of the plate in the end boundary conditions. This occurs, in part, due to the teflon tape that is necessary to prevent the introduction of extraneous load. The measured end-shortening displacements were approximately twice as compliant as predicted and had very large coefficients of variation, leading to questions concerning their validity. Therefore, these data are not reported herein.

A better technique to measure this effective modulus parameter is needed. It is suggested that an optical technique could be used to measure the in-plane deflection. This would eliminate the problem due to nonuniform load as well as that due to compliance in the loading system.

The experimentally observed and theoretically predicted primary buckling loads for the laminates are summarized in Table 4. In general, the buckling loads determined via the Southwell method showed the same trends as those calculated analytically. However, in almost all cases the experimental results actually exceed the predicted buckling loads. Additionally, there was virtually no distinguishable difference between the experimental buckling loads for the two types of side boundary conditions, although the analysis indicates an increase in buckling load ranging from 10% to nearly 60% for laminates with clamped sides over those with simply supported sides.

This supports the concept that the bifurcation buckling load serves little purpose except to give some quick comparison of various laminates. This is further exemplified by the fact that the experimental buckling load does not correspond to any meaningful location on the load vs deflection curves (such as those later shown). Thus, this calculation may be used to rank the laminates, but the nonlinear solution is necessary to describe the actual behavior and to quantify the load-deflection response.

These calculations did, however, demonstrate that the modes assumed for the Rayleigh-Ritz technique were sufficient to

Table 4 Primary buckling loads[a]

	Clamped sides			Simply supported sides		
Laminate	Experiment	Rayleigh-Ritz	Finite-element	Experiment	Rayleigh-Ritz	Finite-element
$[0_3/90_3]_s$	5.6(17%)[b]	8.6	8.5	7.1	7.3	7.2
$[0_3//90_3//90_3//0_3]_T$	11.5(20%)	9.8	9.8	11.9	8.4	8.3
$[0_3//90_3//0_3//90_3]_T$	9.8(20%)	8.2	8.3	6.6	5.2	5.3
$[0_2//45_2//0_2//45_2//0_2]_T$	7.4(21%)	6.0	5.9	6.1	5.3	5.2
$[0_2//45_2//0_2//-45_2//0_2]_T$	6.6(26%)	5.5	5.4	7.9	5.0	4.9

[a]All values in kN.
[b]Numbers in parentheses are coefficients of variation.
[c]Only one specimen of each type tested with simply supported sides.

properly represent the first-mode behavior. This can be concluded since the linear Rayleigh-Ritz and the linear finite-element solution are virtually identical. Thus, the nonlinear Rayleigh-Ritz technique, which uses the same modes, should correlate well with the experimental observations as subsequently discussed.

B. Postbuckling Behavior

Aside from the more subtle deflection components caused by the various elastic couplings, two general types of postbuckling behavior were observed on a global scale. Most of the laminates exhibited a primary global bending mode throughout the entire range of compressive loading, beginning with the application of the load and continuing to failure, as illustrated in Figs. 4–6. However, two unsymmetric laminates transitioned either smoothly or with a snap into a secondary buckling mode, as shown in Fig. 7. Components of twisting and higher bending modes were often superimposed on the deflection patterns.

In all cases, the tests were conducted to failure. However, the failure mode that occurred is a consequence of the construction process used for the unsymmetric laminates. None of the laminates exhibited any fiber breakage. Failure occurred via delamination at the room temperature bondline, followed by matrix cracking and a sudden decrease in load-carrying capability. This delamination is not a true measure of the ultimate load-carrying capability of the laminate, since this construction has less resistance to delamination than a laminate cured in one step. Accordingly, the calculations of the laminate behavior via the nonlinear Rayleigh-Ritz technique were accomplished at 4.5 kN intervals up to 27.0 kN, which was within ±30% of the failure load of all the test specimens.

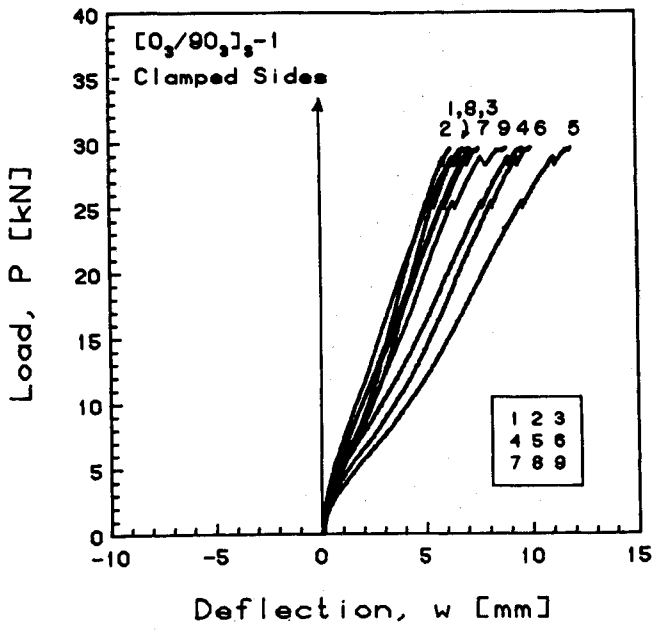

Fig. 4 Experimental load-deflection plot for $[0_3/90_3]_s$ specimen with clamped sides.

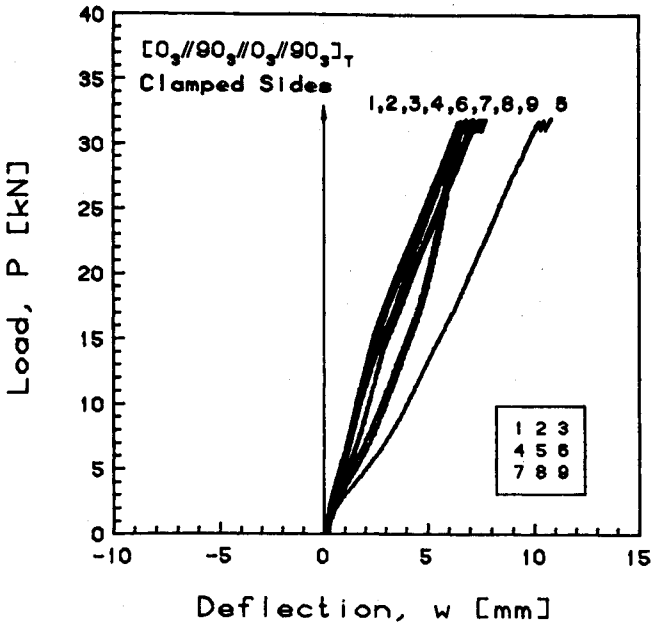

Fig. 6 Experimental load-deflection plot for $[0_3//90_3//0_3//90_3]_T$ specimen with clamped sides.

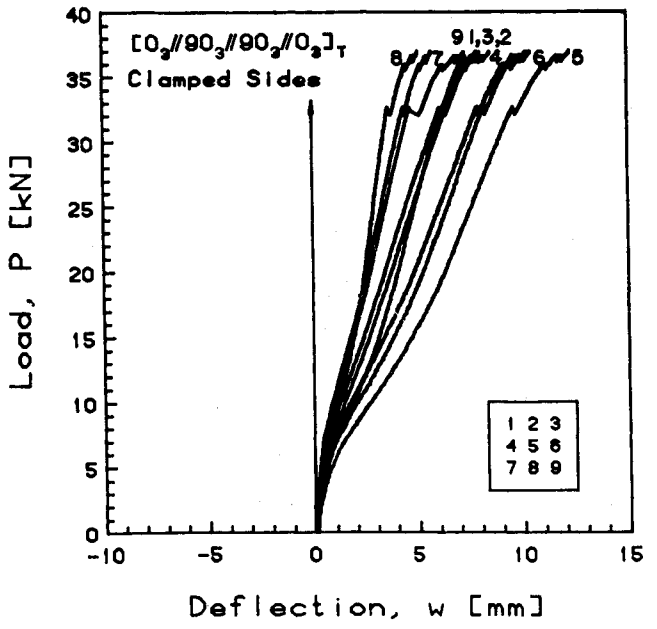

Fig. 5 Experimental load-deflection plot for $[0_3//90_3//90_3//0_3]_T$ specimen with clamped sides.

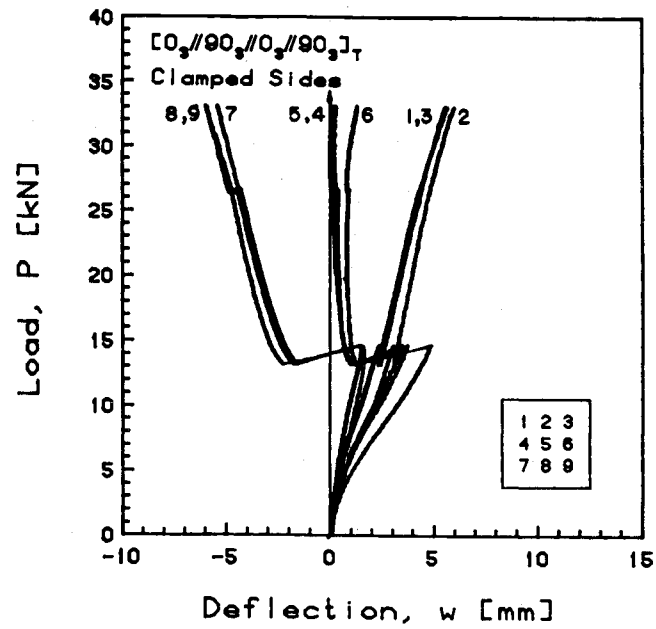

Fig. 7 Experimental load-deflection plot for $[0_3//90_3//0_3//90_3]_T$ specimen with clamped sides showing secondary buckling.

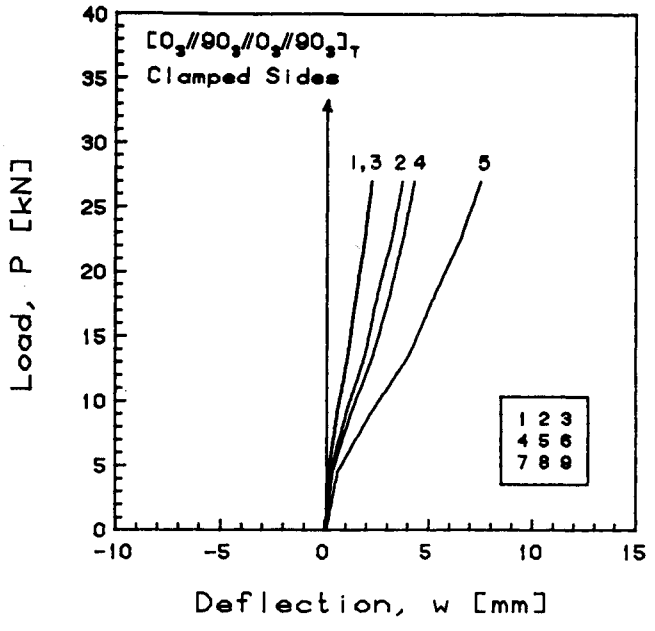

Fig. 8 Analytical load-deflection plot for $[0_3//90_3//0_3//90_3]_T$ specimen with clamped sides.

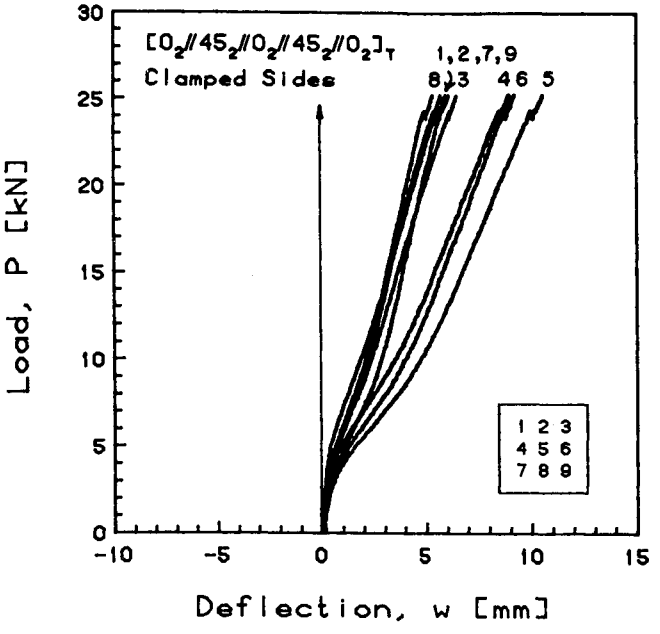

Fig. 10 Experimental load-deflection plot for $[0_2//45_2//0_2//45_2//0_2]_T$ specimen with clamped sides.

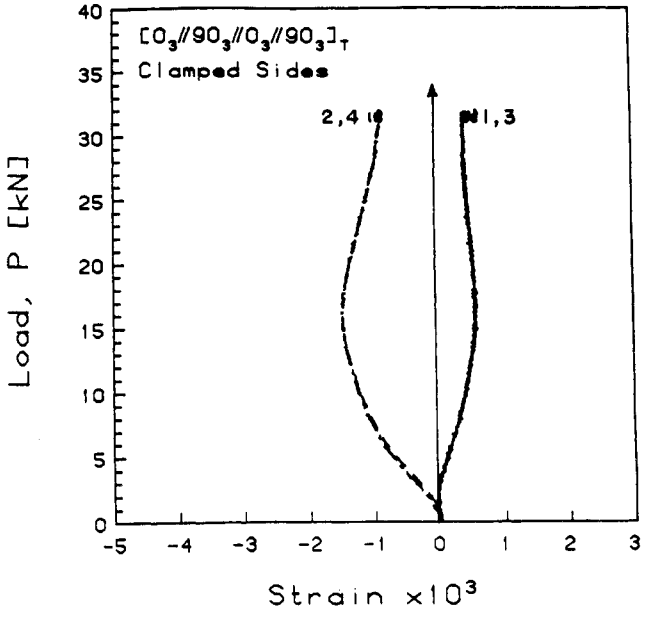

Fig. 9 Experimental load-strain plot for $[0_3//90_3//0_3//90_3]_T$ specimen with clamped sides indicating formation of third mode.

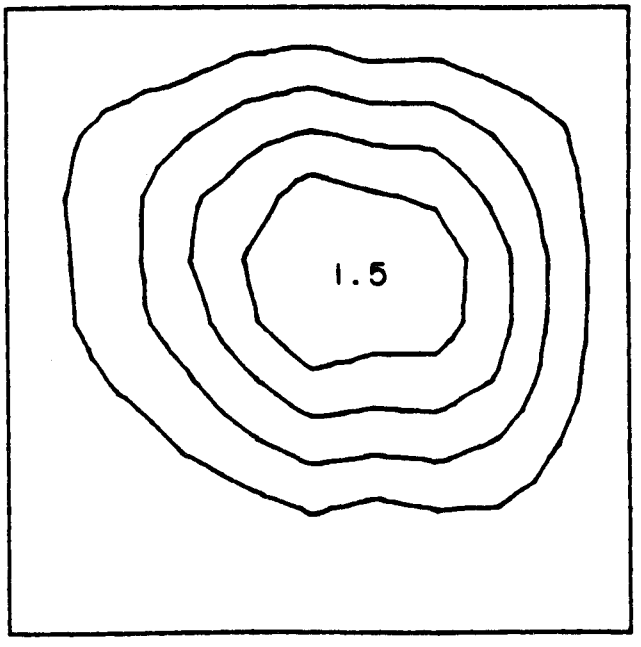

Fig. 11 Experimental isodeflection contour of $[0_2//45_2//0_2//45_2//0_2]_T$ specimen with clamped sides at 3.7 kN indicating twisting (number in center is center deflection in mm).

1. Room Temperature Bondline

The effect of the room temperature bondline is assessed by comparing the behavior of the $[0_3/90_3]_s$ and $[0_3//90_3//90_3//0_3]_T$ laminates presented in Figs. 4 and 5. The increased thickness due to the bondlines stiffens this laminate by increasing the moment of inertia without changing the basic characteristics of the laminate's behavior. This can be properly accounted for in the analysis by modeling the bondline as an additional ply with the properties of the adhesive shown in Table 2. Thus, this is a valid experimental technique to obtain flat unsymmetric laminates and to investigate their prefailure behavior.

2. Bending-Stretching Coupling

The $[0_3//90_3//0_3//90_3]_T$ laminates were manufactured from sublaminates nominally identical to those used in the $[0_3//90_3//90_3//0_3]_T$ laminates, but with an antisymmetric stacking arrangement. This resulted in lower longitudinal bending stiffness, higher transverse bending stiffness, and, most importantly, the introduction of coupling between bending and stretching. The $[0_3//90_3//0_3//90_3]_T$ laminate was initially less stiff than the $[0_3//90_3//90_3//0_3]_T$ arrangement. This is attributable to the lower longitudinal bending stiffness and was further manifested at higher loads.

A more dramatic effect was noted in two of the laminates that buckled into a second longitudinal buckling mode, as evidenced in Fig. 7. This was not predicted by the nonlinear analysis shown in Fig. 8, although the nonlinear analysis did correlate well with the plates, which did not snap into the second mode, as seen in Fig. 6. Further examination of these

results, however, reveals that a third mode began to form in these plates, as evidenced in Fig. 6, by the slight reversal in the deflection trend at locations 4 and 6. A further demonstration of the beginning of this third mode superimposed on the global first mode can be seen in the stress-strain curve for that $[0_3//90_3//0_3//90_3]_T$ laminate presented in Fig. 9. The strain gages, located slightly offset from the center of the plate, show a reduction in the strain magnitude, indicating that they are located in local deflection pockets or dimples. This corresponds to the reversal in transducers 4 and 6 and is indicative of local dimpling due to the impending onset of a third axial bending-mode component. This is in direct contrast to the behavior of the similar specimens that buckled into a second mode where the stress-strain behavior also showed a snap behavior, reducing these strains to nearly zero with no change in their values with further increase in loading.

The notably different behavior of nominally identical laminates indicates that unsymmetric laminates, especially those with bending-stretching coupling, are very sensitive to any eccentricities or disturbances and have at least two stable equilibrium positions for some loads. The path that is followed apparently depends upon the specific conditions as the plate passes through a critical region.

3. Twisting and Shearing Couplings

The stretching-shearing and bending-twisting couplings are present in the $[0_2//45_2//0_2//45_2//0_2]_T$ laminates and introduce shearing and twisting into the deflection pattern. These are not readily observable in the load-deflection plot of Fig. 10, but they can be clearly identified in the isodeflection contour map for this laminate in Fig. 11 where the isodeflection lines are twisted due to these couplings.

The similar laminate type with one of the 45_2 sublaminates reversed to form a $[0_2//45_2//0_2//-45_2//0_2]_T$ configuration showed very similar load-deflection results, as illustrated in Fig. 12. This occurs despite the fact that this laminate has extension-twisting coupling that the $[0_2//45_2//0_2//45_2//0_2]_T$ configuration does not. This can be reconciled by realizing that the stretching-shearing coupling response of the $[0_2//45_2//0_2//45_2//0_2]_T$ laminate is linked to its bending-twisting coupling response, since the geometrically nonlinear behavior for large deflections couple together the in-plane and out-of-plane behavior. Thus, these two laminates effectively have the same couplings.

4. Boundary Conditions

In general, the behavior of the laminates with simply supported sides was very similar to the behavior of the laminates tested with clamped side boundary conditions. The characteristics were very much the same, but the simply supported side boundary conditions allowed larger magnitude out-of-plane deflections. This can be seen in Fig. 13 for the $[0_3//90_3//0_3//90_3]_T$ laminate, as contrasted to the behavior in Fig. 7 for the case of this laminate with clamped side boundary conditions.

The nonlinear Rayleigh-Ritz analysis predicted the behavior of the laminates with simply supported side boundary conditions extremely well, as may be seen by comparing Figs. 13 and 14. The analysis underestimated the actual deflections for the clamped case. This is because the actual side boundary conditions are not truly clamped, and the analysis models only a finite number of degrees of freedom and is, therefore, inher-

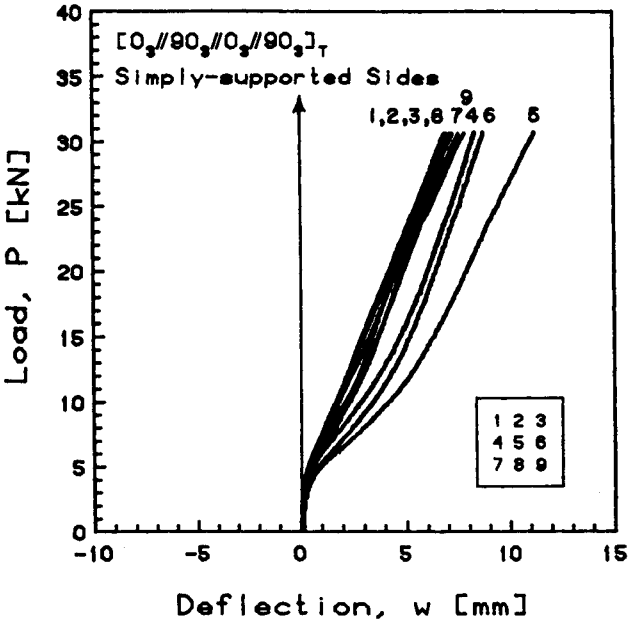

Fig. 13 Experimental load-deflection plot of $[0_3//90_3//0_3//90_3]_T$ specimen with simply supported sides.

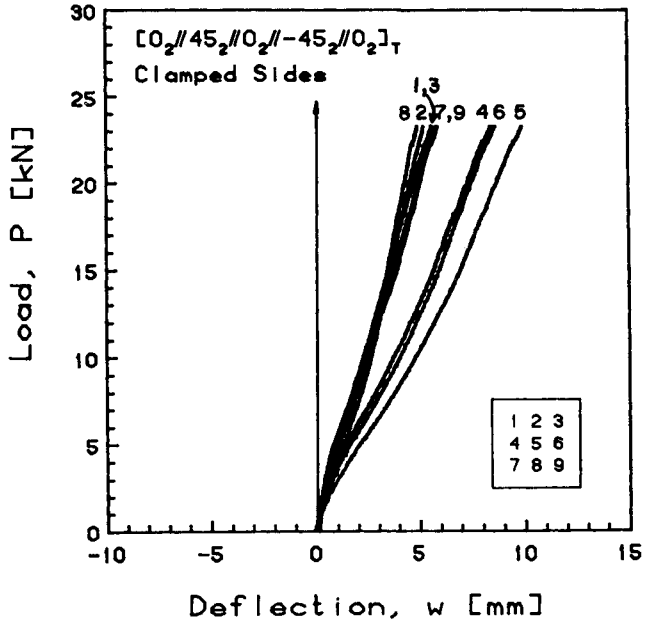

Fig. 12 Experimental load-deflection plot of $[0_2//45_2//0_2//-45_2//0_2]_T$ specimen with clamped sides.

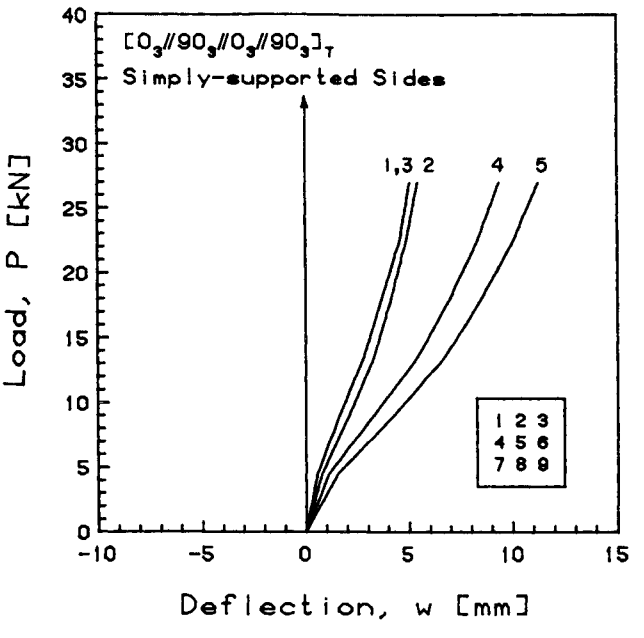

Fig. 14 Analytical load-deflection plot of $[0_3//90_3//0_3//90_3]_T$ specimen with simply supported sides.

ently too stiff. In spite of these limitations, the analytical predictions match the experimental observations reasonably well in almost all cases except where a secondary buckling mode occurred.

Another effect of the boundary conditions is their interaction with the elastic couplings. The more restrictive the boundary conditions are, the greater the influence of the coupling terms. More restrictive boundary conditions prohibit natural deflections at the edges and, thus, introduce stresses that amplify the effects of the couplings.

VI. Summary

This experimental and analytical investigation conducted on the buckling and postbuckling behavior of graphite/epoxy laminates with various elastic couplings has shown that mechanical couplings, especially those included in the generic category of membrane-flexural coupling, have profound effects on the behavior of the laminates. These couplings reduce the predicted and observed buckling loads (as determined via the Southwell method). However, the classical bifurcation load does not necessarily correspond to any meaningful physical phenomenon for laminates with membrane-flexural coupling, since lateral deflections begin simultaneously with the application of compressive load due to the effects of these couplings. Thus, a full nonlinear analysis must be performed in order to fully quantify the behavior of unsymmetric laminated plates.

It has also been shown that bending-stretching coupling can cause laminated plates to buckle into a secondary mode. However, nominally identical plates do not necessarily show the same behavior, since the $[0_3//90_3//0_3//90_3]_T$ laminates exhibit both primary bending until failure as well as a snap into a second mode. This indicates that there are at least two stable equilibrium configurations beyond the second critical buckling load. A critical region exists in the vicinity of this load where local disturbances and eccentricities determine which path the plate will follow. Beyond this critical region, the plate stiffens geometrically in either path, stabilizing the plate and preventing the snap-through phenomenon from recurring. Furthermore, these plates show the initiation of a local third mode at high loads and deflections, as manifested by a dimple at the plate center.

The $[0_2//45_2//0_2//45_2//0_2]_T$ laminate that has stretching-shearing and bending-twisting coupling behaves nearly identically to the $[0_2//45_2//0_2//-45_2//0_2]_T$ laminate in which there is a coupling between the stretching and twisting. This is especially true at higher loads and is a result of the linkage of the stretching-shearing and bending-twisting behaviors by the geometric nonlinearities caused by the large deflections typical in the postbuckling range.

The effects of these elastic couplings are increased as the side boundary conditions become more restrictive, since restraining the boundaries prohibits the natural deflections at the edges. This restriction introduces stresses which, in turn, amplify the effects of the coupling mechanisms.

The linear analysis used herein was capable of ranking laminates in terms of their initial resistance to out-of-plane deflection. However, the nonlinear analysis was necessary to quantify the deflections in the postbuckling region. Further attention should focus on properly modeling the deflection patterns that result, especially the second and third modes that formed and were not modeled/predicted by the current analytical technique.

Acknowledgments

Support for this work was provided by the Boeing Military Airplane Company under Contract BMAC P.O. AA0045. The authors wish to gratefully acknowledge the invaluable assistance offered by John Dugundji of the Department of Aeronautics and Astronautics at the Massachusetts Institute of Technology.

References

[1]Jensen, D. W., Crawley, E. F., and Dugundji, J., "Vibration of Cantilevered Graphite/Epoxy Plates with Bending-Torsion Coupling," *Journal of Reinforced Plastics and Composites*, Vol. 1, July 1982, pp. 254–269.

[2]Sherrer, V. C., Hertz, T. J., and Shirk, M. H., "Wind Tunnel Demonstration of Aeroelastic Tailoring Applied to Forward Swept Wings," *Journal of Aircraft*, Vol. 18, Nov. 1981, pp. 976–983.

[3]Dastin, S., Eidinoff, H. C., and Arman, H. Jr., "Some Engineering Aspects of the X-29 Airplane," *Proceedings of the 28th National SAMPE Symposium*, SAMPE, Covina, CA, April 1984, pp. 1483–1449.

[4]Cristescu, N., Malvern, L. E., and Sierakowski, R. L., "Failure Mechanisms in Composite Plates Impacted by Blunt-Ended Penetrators," *Foreign Object Impact Damage to Composites*, American Society for Testing and Materials, ASTM STP 568, 1975, pp. 159–172.

[5]Leissa, A. W., "Buckling of Laminated Composite Plates and Shell Panels," Air Force Wright Aeronautical Labs., AFWAL-TR-85-3069, June 1985.

[6]Reissner, E. and Stavsky, Y., "Bending and Stretching of Certain Types of Heterogeneous Elastic Plates," *Journal of Applied Mechanics*, Vol. 9, Sept. 1961, pp. 402–408.

[7]Kicher, T. P. and Mandell, J. F., "A Study of the Buckling of Laminated Composite Plates," *AIAA Journal*, Vol. 9, April 1971, pp. 605–613.

[8]Lagace, P. A., Jensen, D. W., and Finch, D. C., "Buckling of Unsymmetric Composite Laminates," *Composite Structures*, Vol. 5, No. 2, 1986, pp. 101–123.

[9]Chia, C. Y., *Nonlinear Analysis of Plates*, McGraw-Hill, New York, 1980.

[10]Jensen, D. W., "Buckling and Postbuckling Behavior of Unbalanced and Unsymmetric Laminated Graphite/Epoxy Plates," Technology Lab. for Advanced Composites, Rept. 86-3, Ph.D. Thesis, Massachusetts Institute of Technology, Cambridge, MA, Jan. 1986.

[11]Sumihara, K., "Thin Shell and New Invariant Elements by Hybrid Stress Method," Ph.D. Thesis, Massachusetts Institute of Technology, Cambridge, MA, June 1983.

[12]Pian, T. H. H., "Finite Elements Based on Consistently Assumed Stresses and Displacements," *Finite Elements in Analysis and Design*, Vol. 1, April 1985, pp. 131–140.

[13]von Kármán, T., *Encyklopaedie der Mathematischen Wissenschaften*, Vol. IV, 1910, p. 349.

[14]Zhang, Y. and Matthews, F. L., "Postbuckling Behavior of Anisotropic Laminated Plates Under Pure Shear and Shear Combined with Compression Loading," *AIAA Journal*, Vol. 22, Feb. 1984, pp. 281–286.

[15]Southwell, R. V., "On the Analysis of Experimental Observations in Problems of Elastic Stability," *Proceedings of the Royal Society of London*, Ser. A, Vol. 135, London, 1932, pp. 601–616.

[16]Minguet, P., "Etude du Comportement Postcritique de Panneaux en Materiaux Composites," B.S. Thesis, Université de Liège, Liège. Belgium, 1984.

[17]Ashton, J. E. and Love, T. S., "Experimental Study of the Stability of Composite Plates," *Journal of Composite Materials*, Vol. 3, April 1969, pp. 230–242.

[18]Finch, D. C., "The Buckling of Symmetric and Unsymmetric Composite Plates with Various Boundary Conditions," Technology Lab. for Advanced Composites, Rept. 84-3, S.M. Thesis, Massachusetts Institute of Technology, Cambridge, MA, Feb. 1984.